Supplementary Material for
Observation of superparamagnetism in coexistence with quantum anomalous Hall C=±1 and C=0 Chern states

Ella O. Lachman[1], Masataka Mogi[2], Jayanta Sarkar[1] Aviram Uri[1], Kousik Bagani[1], Yonathan Anahory[1,3], Yuri Myasoedov[1], Martin E. Huber[4], Atsushi Tsukazaki[5], Masashi Kawasaki[2,6], Yoshinori Tokura[2,6] and Eli Zeldov[1]

[1]Department of Condensed Matter Physics, Weizmann Institute of Science, Rehovot 7610001, Israel

[2]Department of Applied Physics and Quantum Phase Electronics Center (QPEC), University of Tokyo, Tokyo 113-8656, Japan

[3]Racah Institute of Physics, The Hebrew University, Jerusalem 9190401, Israel

[4]Department of Physics, University of Colorado Denver, Denver, Colorado 80217, USA

[5]Institute for Materials Research, Tohoku University, Sendai, 980-8577, Japan

[6]RIKEN Center for Emergent Matter Science (CEMS), Wako, 351-0198, Japan

e-mail: eli.zeldov@weizmann.ac.il, ella.lachman@weizmann.ac.il

1. SQUID-on-tip characteristics

The SOT used for magnetic imaging (Fig. 1c) was fabricated by three-step deposition of Indium onto a pulled quartz pipette following the methods in Refs. 35-37. Figure S1 shows the quantum interference pattern of the critical current $I_c(H)$ with a period of 0.2 T corresponding to the effective diameter of the SOT of 115 nm.

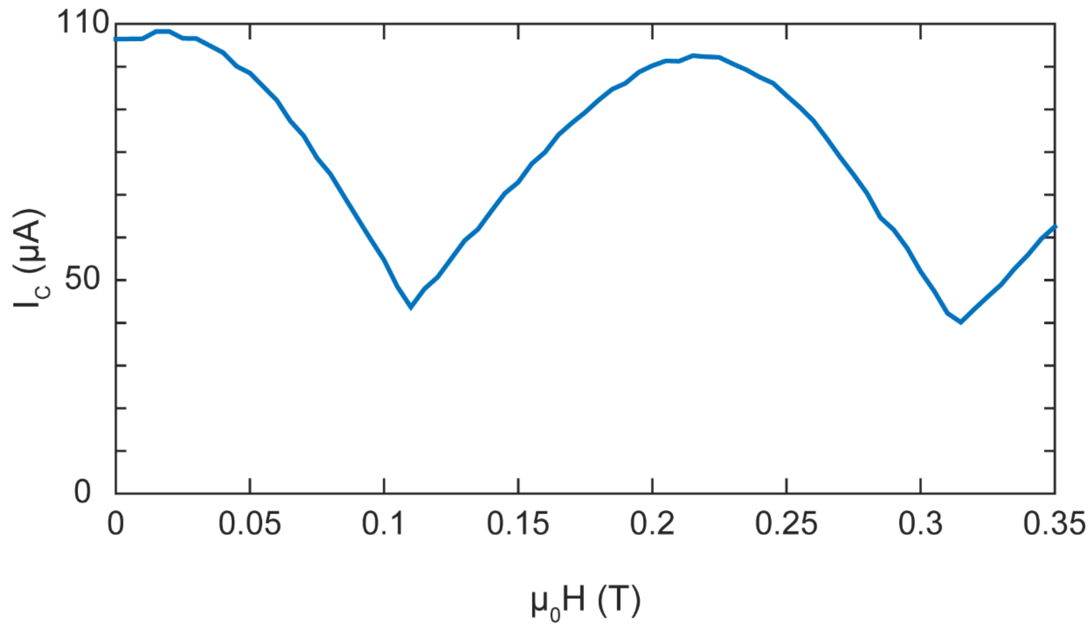

Figure S1. SQUID-on-tip critical current as a function of applied magnetic field at $T = 300$ mK. The period of the $I_c(H)$ interference pattern is 0.2 T, corresponding to a loop diameter of 115 nm.

2. Movie of the SPM islands reversal dynamics

The scanning magnetic images of $B_z(x,y)$ were acquired simultaneously with the transport coefficients upon increasing the applied field at constant increments of 0.2 mT. Movie S1 shows a compilation of a sequence of such $B_z(x,y)$ images and of the differences between the consecutive images $\Delta B_z(x,y)$ in the vicinity of the coercive field $\mu_0 H_c = 137$ mT, revealing the dynamics of the SPM island reversal process. A frame from the movie is described in Fig. S2. As can be seen from the $\Delta B_z(x,y)$ image sequence, the magnetization reversal process occurs through isolated flipping events, appearing as bright green/red peaks revealing the islands that reversed their magnetization from $-m_i$ to $+m_i$ as the field was incremented by 0.2 mT. The flipping events are uncorrelated in space indicating weak coupling between the neighboring SPM islands. The revealed dynamics is distinctly different from the correlated domain wall propagation in FM films. In particular, no domain wall can be defined in $B_z(x,y)$ or $\Delta B_z(x,y)$ images and no propagating front is observed at any value of the applied field. The simultaneously acquired transport coefficients (Figs. S2c,d) show a peak in R_{xx} at the coercive field and a zero crossing in R_{xy}.

Since we are interested in the analysis of the local field arising from the film magnetization the trivial increase in the background field due to the incremental change in the applied field was removed for clarity by subtracting the median value of the signal in the ten left-most columns (500 nm) in the $B_z(x,y)$ images. Since the stray field of the magnetic structure decays rapidly away from the edge of the film, at this location of 3 μm away from the film edge the local field is essentially constant and is approximately equal to the value of the applied field.

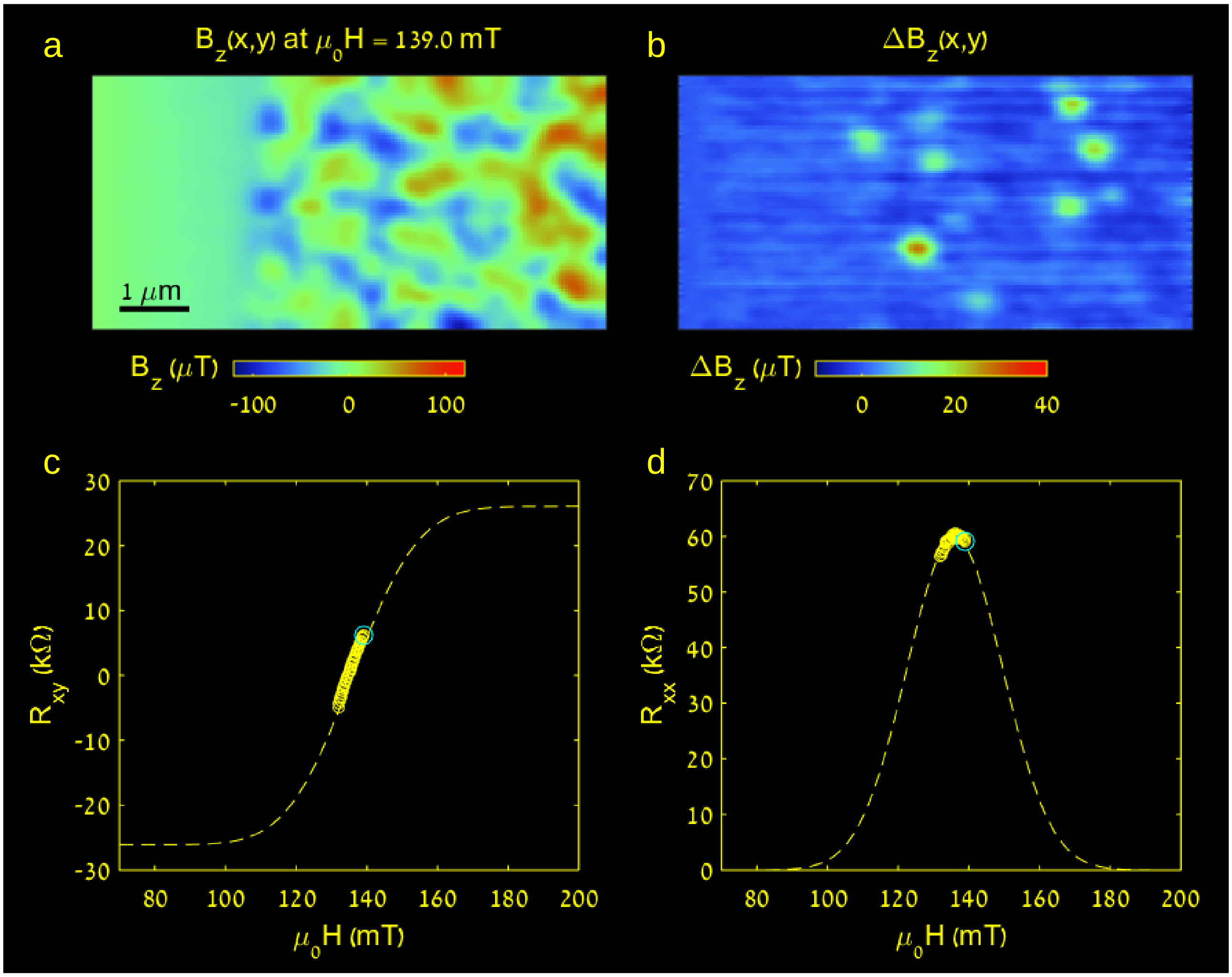

Figure S2. Frame from Movie S1 – magnetization reversal process in modulation doped Cr-(Bi,Sb)$_2$Te$_3$ film at $T = 300$ mK. (**a**) Scanning SOT image 4 × 8 μm^2 of the out-of-plane magnetic field $B_z(x,y)$ at ~300 nm above the sample surface. The running title indicates the value of the applied field incremented in steps of 0.2 mT between consecutive images. Pixel size 50 nm, scan rate 9 μm/sec. (**b**) Differential image $\Delta B_z(x,y)$ obtained by subtracting the preceding $B_z(x,y)$ image from the current one in (**a**). Isolated magnetic reversal events of the SPM islands in the direction of the ascending applied field are visible as red-green $\Delta B_z(x,y)$ peaks appearing at random locations within the film. The spatial extent of these peaks is determined by the size of the SOT (115 nm) and by its scanning height above the sample, while the physical size of the flipping SPM islands can be derived from the intensity of the $\Delta B_z(x,y)$ peaks (see Fig. 2). (**c**) R_{xy} of the sample measured simultaneously with the magnetic imaging. The blue circle shows the current value while the yellow circles are the data at previous field values. The dashed line is a guide to the eye of the full R_{xy} trace through the plateau transition. (**d**) Same as (**c**) for R_{xx}.

3. Analysis of SPM dynamics in the vicinity of the incipient $C = 0$ state

In order to follow the evolution of the magnetization transition we derived the magnetic moment $2m_i$ of each detected SPM island reversal event in the entire sequence of $\Delta B_z(x, y)$ images as described in Fig. 2. By summing the $2m_i$ values we obtain the net change in the magnetic moment ΔM in each $\Delta B_z(x, y)$ image due to field increment of 0.2 mT. Figure S3a shows the dependence of ΔM on increasing applied field (color dots, left axis). A measurable rate of the SPM island reversals ΔM is observed from fields as low as 40 mT (our lowest studied field). As the field approaches the coercive field $\mu_0 H_c = 137$ mT a large increase in ΔM is attained over a range of magnetic fields followed by a decrease above 160 mT. A lower but a finite ΔM reversal rate persists up to our highest studied field of 262 mT which is almost twice $\mu_0 H_c$. This result shows that even though the global average coercive field is rather well defined, the coercive field of the individual SPM islands has a very broad distribution.

Since the hold time of our ^{3}He cryostat was insufficient for performing the SOT imaging studies in a single run over the entire field span, each field range was measured in a separate run as indicated by the different colors in Figs. 2f,h and S3. In each run the applied field was first ramped at a rate of $d\mu_0 H/dt = 400$ mT/min from $\mu_0 H = -1$ T to the desired field and then a sequence of magnetic images and concurrent transport coefficients was acquired at a much slower effective sweep rate of 40 μT/min. The SPM state displays slow but finite time relaxation even at our base temperature of 300 mK. As a result, after the initial fast field ramp the first few measurement points show a slightly faster evolution of the signal as visible in the small initial mismatch in the transport coefficients between the different field ranges in Fig. S3b. To account for the faster initial time relaxation we therefore chose the different field ranges to overlap partially to attain data continuity. In field range around 200 mT no magnetic data could be acquired because of the poor SOT sensitivity in the "blind region" due to the periodic nature of the quantum interference pattern (Fig. S1). Another narrow "blind region" was present around $\mu_0 H = 100$ mT (yellow data range in Fig. S3) through which the field was ramped at a faster rate of 200 μT/min, resulting in the observed kink in the σ_{xx} data in Fig. S3a.

In order to derive the overall magnetization behavior we calculated the total magnetic moment $M(H)$ by integration of the ΔM values over the field increments within each field range. The full $M(H)$ curve (Fig. S3a, color lines, right axis) was then attained by matching the data of the field segments and defining $M(H_c) = 0$. The resulting $M(H)$ describes the overall transition of the magnetic moment within our 4×8 μm^2 imaging window.

Figure S3b shows the corresponding transport coefficients measured simultaneously with the magnetic imaging. A minimum in σ_{xx} and a plateau like feature in σ_{xy} are clearly visible in the vicinity of the coercive field $\mu_0 H_c = 137$ mT indicating the incipient $C = 0$ state. As discussed in the main text, in order to attain a robust $C = 0$ axion state the difference between the coercive fields of the two magnetically doped layers ΔH_c should be substantially larger than the width of the magnetic transition δH_c of each of the layers. The fact that ΔM shows a single broad range of enhanced SPM reversals rather than two peaks at the two coercive fields and that the corresponding $M(H)$ shows a continuous increase with no clear intermediate plateau around $M = 0$ indicate that the width of each transition δH_c is comparable or larger than ΔH_c. As a result, the axion state with a full ZHP cannot be developed.

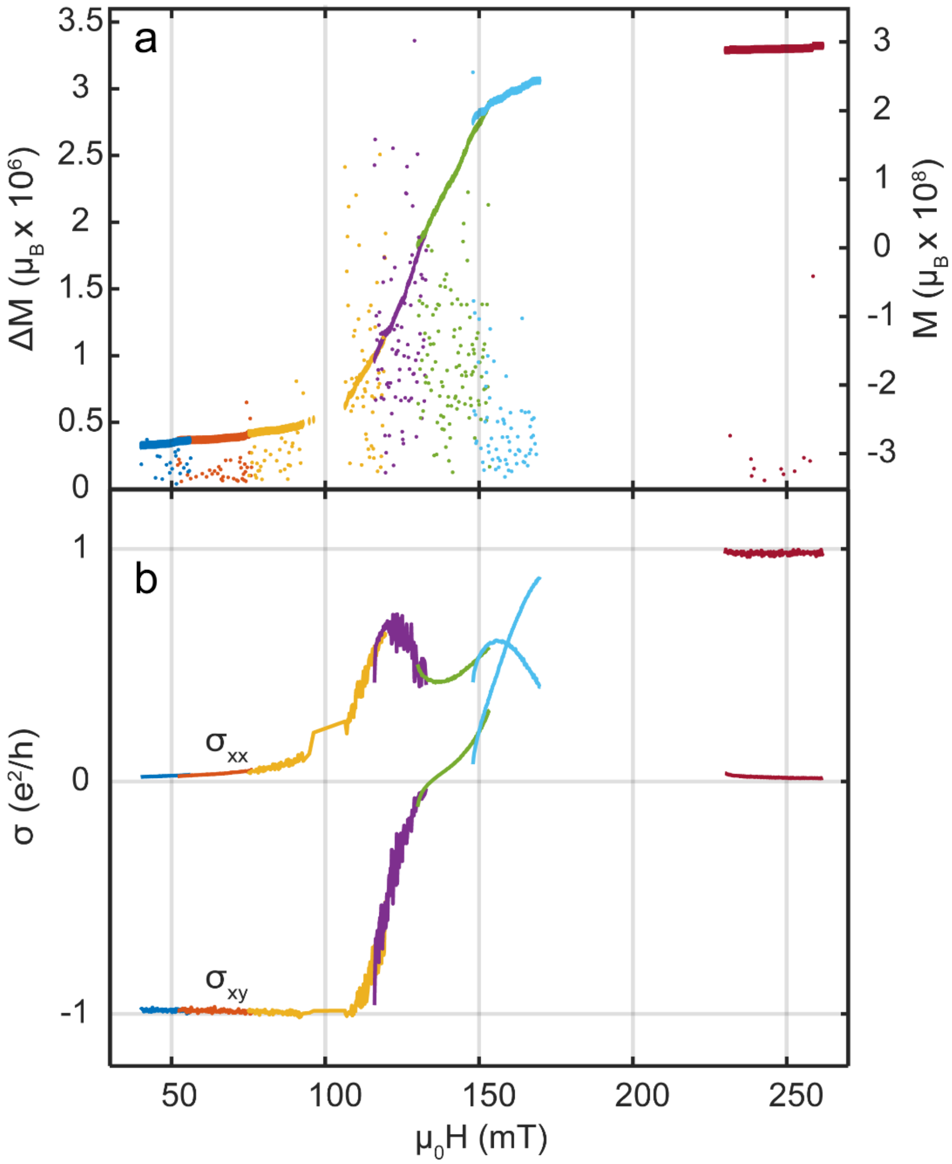

Figure S3. SPM magnetization dynamics and simultaneous transport measurements vs. applied field. (**a**) The total change in magnetic moment ΔM derived from SPM island reversals in each $\Delta B_z(x, y)$ image (color dots, left axis), and the cumulative magnetic moment M (color lines, right axis) as a function of increasing applied field. (**b**) Simultaneously acquired transport coefficients showing an incipient $C = 0$ state indicated by a dip in σ_{xx} and a kink in σ_{xy} near the coercive field.

4. Temperature dependence of the transport coefficients in $C = 0$ and $C = \pm 1$ states

The absence of sufficient alignment of the SPM islands in the incipient $C = 0$ axion state should also affect its stability with respect to temperature. In order to test this we have performed transport studies in a dilution refrigerator on a second sample (Sample 2) of similar structure and composition. Figure S4 shows the field dependence of σ_{xx} and σ_{xy} and of σ_{xx} vs. σ_{xy} at a number of temperatures from $T =$ 50 mK to 300 mK. The features associated with the $C = 0$ state diminish faster with increasing T as compared to $C = \pm 1$ characteristics. In particular, the plateau-like $C = 0$ feature in σ_{xy} in Fig. S4b is almost entirely washed out when the temperature is increased to 270 mK (yellow curve) while σ_{xy} remains nearly fully quantized in the $C = \pm 1$ QAH plateaus. Similarly, the $C = 0$ dip in σ_{xx} in Figs. S4a and S4c is substantially reduced at $T =$ 250 mK (green curve) as compared to 70 mK (light blue) while σ_{xx} remains close to zero in the QAH plateaus. There results point to the dominant role of the SPM order and the degree of island alignment on the stability of $C = 0$ and $C = \pm 1$ states.

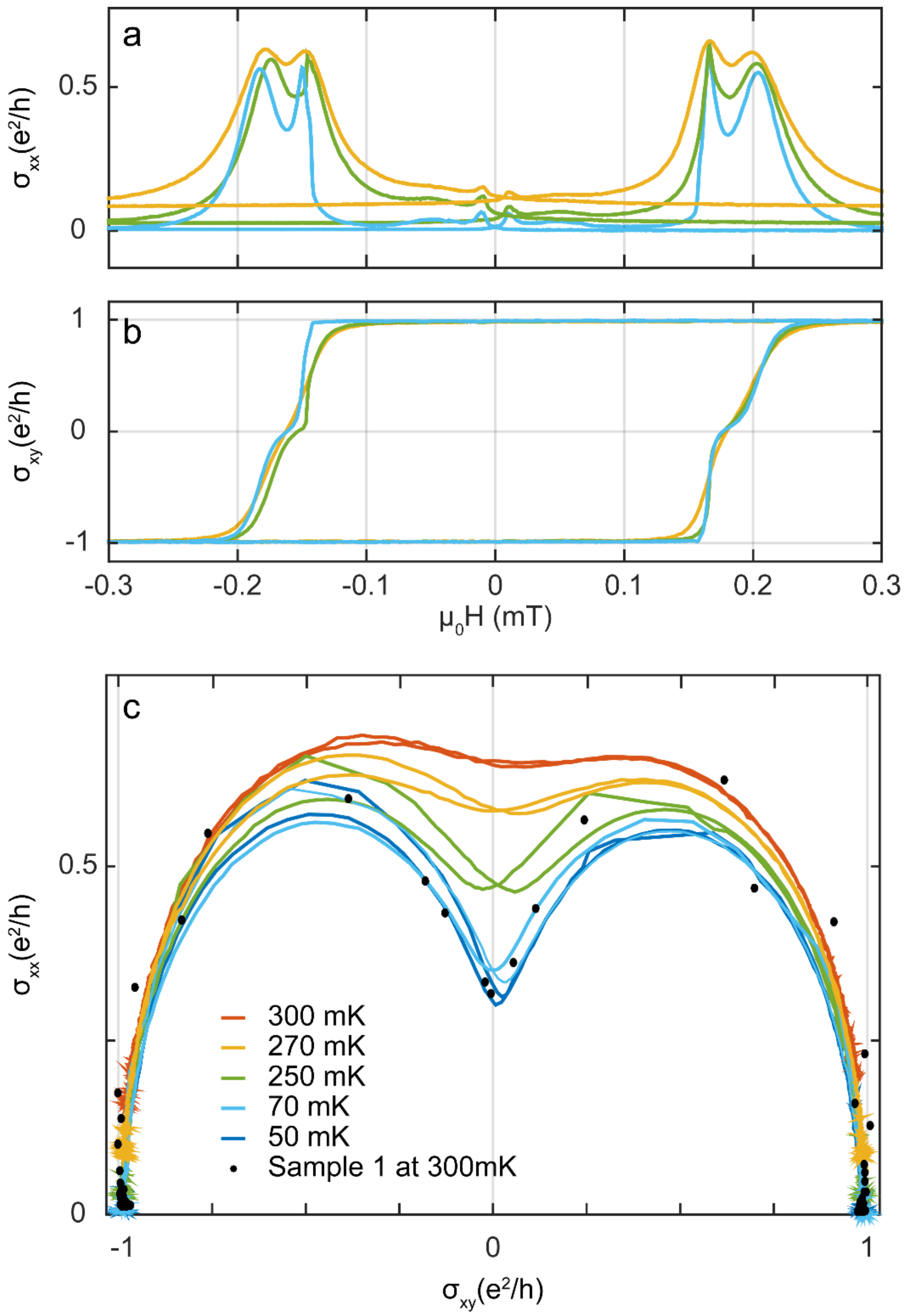

Figure S4. Transport measurements of modulation doped Cr-(Bi,Sb)$_2$Te$_3$ Sample 2 at different temperatures. σ_{xx} (**a**) and σ_{xy} (**b**) as a function of the applied field and σ_{xx} vs. σ_{xy} (**c**) showing the QAH state with full quantization and the insipient $C = 0$ state at indicated temperatures. The black dots in (**c**) show for comparison the $T = 300$ mK values in Sample 1 of the main text.